ARTICLE INFO

Article ID: 14-15-03-0013

doi:10.4271/14-15-02-0013

Assessing Geographical and Seasonal Influences on Energy Consumption and Driving Range for Electric Drayage Trucks

Ankur Shiledar,[1] Manfredi Villani,[1] Joseph N. E. Lucero,[2] Ruixiao Sun,[3] Vivek A. Sujan,[3] Simona Onori,[4] and Giorgio Rizzoni[1]

[1]The Ohio State University, Department of Mechanical and Aerospace Engineering, USA
[2]Stanford University, Department of Chemistry, USA
[3]Oak Ridge National Laboratory, Building and Transportation Science Division, USA
[4]Stanford University, Department of Energy Science and Engineering, USA

Abstract

The electrification of heavy-duty vehicles is a critical pathway toward improved energy efficiency in the freight sector. The current battery electric truck technology poses several challenges to commercial vehicle operations, such as limited driving range, sensitivity to climate conditions, and long recharging times. Estimating the energy consumption of heavy-duty electric trucks is crucial to assessing the feasibility of fleet electrification and its impact on the electric grid. This article focuses on developing a model-based simulation approach to predict and analyze the energy consumption of electric trucks by considering the impact of weather and geographical conditions on vehicle road load and auxiliary components power consumption, as well as the impact these factors have on driving range. Specifically, drayage trucks employed in logistics around maritime ports are used as a case study, with consideration of seasonal climate variations and geographical characteristics at different locations. The article includes results for three major container ports within the United States, providing region-specific insights into the energy requirements and driving range of the electric drayage trucks in these regions, which will inform decision-makers in integrating electric trucks into the existing drayage operations and plan investments for electric grid development.

History

Received: 25 Feb 2026
Revised: 05 May 2026
Accepted: 08 Jun 2026
e-Available: 29 Jun 2026

Keywords

Electric Trucks, Drayage Fleet, Energy Consumption, Impact of Weather, Seasonal and Geographical Variations, Heavy-duty, Electric Truck Range

Citation

Shiledar, A., Villani, M., Lucero, J., Sun, R. et al., "Assessing Geographical and Seasonal Influences on Energy Consumption and Driving Range for Electric Drayage Trucks," *SAE Int. J. Elect. Veh.* 15(3):2026, doi:10.4271/14-15-02-0013.

ISSN: 2691-3747
e-ISSN: 2691-3755

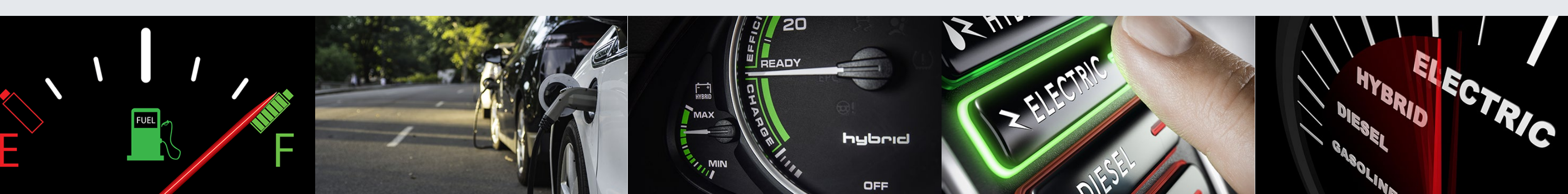

Introduction

Moving goods is crucial to the U.S. economy, with heavy-duty trucks dominating freight movement: 45% of ton-miles, 60% of shipment weight, and 62% of shipment value. Projections show a 50% rise in freight movement by 2050, with trucks playing an even greater role. The trucking industry forms 5.6% of the U.S. GDP, amounting to $1.3 trillion, and employed nearly 2 million drivers for heavy-duty and tractor-trailers in 2021 [1, 2]. Transportation significantly impacts energy use and emissions, being responsible for 23% of global fossil fuel emissions, with the U.S. as a major contributor [3]. Since 2016, transportation has been the top greenhouse gas (GHG) source in the U.S., surpassing electricity [4].

Electrifying heavy-duty vehicles (HDVs) is crucial for reducing transportation energy consumption and enhancing air quality. Full electrification will be gradual and faces various challenges. Switching HDV sales to zero-emission vehicles (ZEVs) will likely take over 20 years [2]. Identifying HDV subgroups, assessing needs, and evaluating if current technology and infrastructure can support ZEV adoption is essential. Some fleets may require additional support to transition to electric models [5, 6]. Current ZEV technology includes battery electric and hydrogen fuel cells, requiring investments in clean energy and charging/fueling networks. The Oak Ridge National Laboratory's OR-AGENT framework has been developed to aid the shift toward electrification by optimizing (i) powertrains, (ii) infrastructure, and (iii) regional energy systems, such as the grid and distributed resources. Figure 1 presents the OR-AGENT workflow. OR-AGENT offers valuable insights for industry stakeholders such as fleet operators and energy providers, supporting HDV applications in specific operation domains. The HDV energy requirements are determined in OR-AGENT through detailed simulations in the "Mission Processing" block (see red box in Figure 1), which uses the vehicle energy consumption model developed in this work.

The focus of this article is the development of high-resolution models for accurate energy consumption estimation of Heavy-Duty Electric Vehicles (HDEVs). The work includes some case studies to showcase the influence of various geographical and weather conditions on the energy consumption and the resulting driving range of electric trucks. For a comprehensive understanding of OR-AGENT, readers are referred to the paper by Sujan et al. [7].

Furthermore, this study focuses on drayage trucks, a specific type of HDV operations. Drayage refers to the transport of freight containers from an ocean port to a destination over short to medium distances (usually below 400 km), commonly referred to as the "first mile" in the logistics industry. HDVs used in drayage applications are usually Class 7 and 8 trucks according to the U.S. Gross Vehicle Weight Rating (GVWR) classification and are predominantly day-cab tractors. A pictorial illustration of drayage operations is presented in Figure 2. Drayage loads typically have departure and arrival points in the same region and do not focus on long-haul movements. Nonetheless, drayage is an integral part of the logistics industry and vital to the overall supply chain management process.

Several major U.S. ports, such as Seattle, New York & New Jersey, Savannah, Houston, Los Angeles, and Long Beach, each in unique regions, exhibit varied seasonal climates and geographical traits. The energy use of ground vehicles is significantly influenced by driver behavior (like acceleration patterns or speed) and environmental conditions [8, 9]. Notably, temperature shifts impact energy needs for heating, ventilation, and air-conditioning (HVAC) systems, especially in electric vehicles,

FIGURE 1 OR-AGENT framework. (Adapted from Ref. [7].) The red box highlights the models developed and presented in this article.

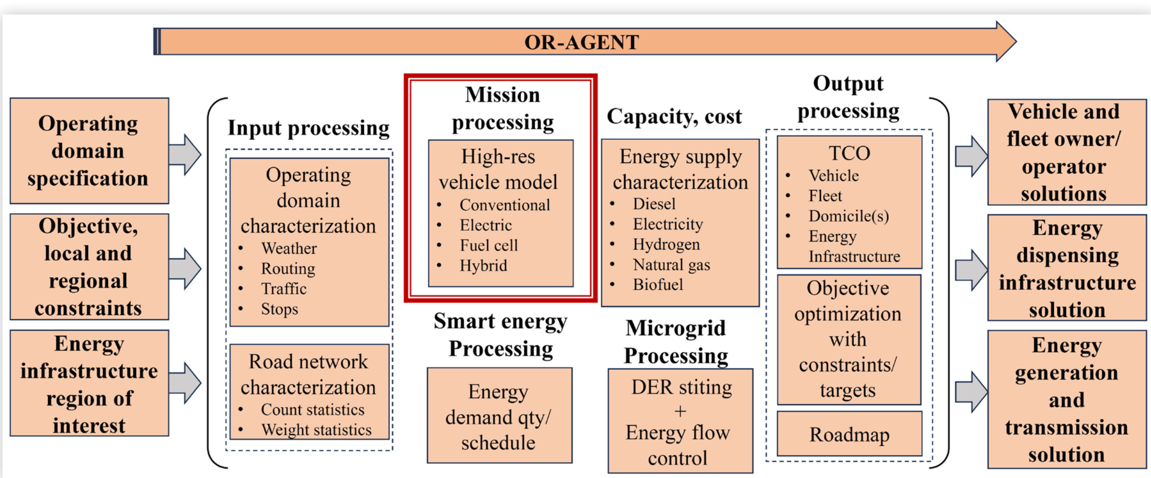

FIGURE 2 Pictorial representation of drayage operations or "first mile" logistics. Containers are shipped using drayage trucks from an ocean port (origin) to a certain distribution hub (destination) over "outbound" routes. Trucks then return to the port, traveling over "inbound" routes.

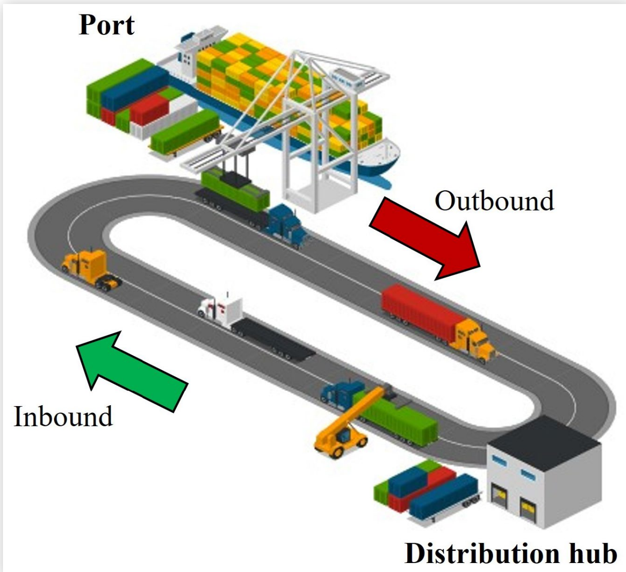

which lack engine waste heat for cabin warming. Extreme temperatures can also degrade battery capacity and lifespan, reducing driving range. Geography impacts energy use through elevation and road grade, often increasing consumption in hilly areas. Consequently, regional energy demand for electric trucks varies, affecting vehicle energy storage design, grid charging demand, and fleet operating costs. This work adopts a bottom-up approach, modeling energy consumption in electric drayage trucks, with a focus on driver habits, seasonal climates, and geographic factors, to support battery electric trucks (BETs) deployment with minimal port disruption. As indicated, BETs' adoption hinges on proving electric powertrains' efficiency and cost competitiveness against diesel engines [10]. A high-resolution vehicle simulator in the OR-AGENT project assesses energy needs in HDVs and addresses research queries like:

- Influence of geography and climate on energy use, driving range, and payload capacity of electric drayage trucks.
- Effect of seasonal energy needs on recharging for the drayage fleet.

This research focuses on drayage operations at the Port of Savannah in Georgia (GA) and extends to the ports of Houston in Texas (TX) and Tacoma in Washington (WA). The regional distinctions in geography and weather across these ports help reveal variations in the energy consumption of electric drayage trucks.

Related Work

In this section, previous research work is reviewed to show how the proposed models and simulations strengthen the state-of-the-art methods for energy consumption evaluation of electric trucks and how this work extends the understanding of electrifying the drayage sector. Previous work in this research area focused on the feasibility of drayage electrification, addressing the following research questions:

- Is state-of-the-art battery technology capable of handling the current drayage fleet operations and allowing a transition to zero-emissions HDVs?
- Can the electric grid support the charging infrastructure?
- What is the overall impact of the deployment of BETs on well-to-wheels emissions?

Tanvir et al. [11] present a well-structured viability assessment of operating an electric drayage fleet in Southern California. Real-world operational data of the current conventional diesel fleet is collected from 20 trucks. Using a virtual vehicle simulator, the electrical energy usage and the battery state-of-charge for BETs are estimated on the real-world collected data. The analysis explored various scenarios with differing assumptions for battery charging and truck scheduling. The results indicate that 85% of the tours could be completed by electric trucks with a 250-kWh battery capacity if charging opportunities are available at the home base during the intervals between the tours. However, the energy consumption model presented in this study is quite simple and based on several assumptions. Despite the efforts of the authors to consider conservative assumptions, their model mostly uses constant climate conditions, component efficiencies, and auxiliary loads, e.g., HVAC, even though this can greatly affect the energy consumption estimation, reducing (or increasing) the percentage of tours that could be served by the electric trucks, therefore limiting the reliability of the results. Also, the model does not seem to account for the geographical characteristics of the region, neglecting the power consumption related to road slope and elevation.

Exhaustive reports on drayage electrification for the Port of New York and New Jersey and on the total cost of ownership for Class 8 tractors have been published by the National Renewable Energy Laboratory (NREL) [12, 13]. NREL researchers used the Future Automotive Systems Technology Simulator (FASTSim) model to estimate the energy consumption of BETs and other vehicle technologies [14]. While FASTSim accounts for road grade, auxiliary loads, and powertrain inefficiencies, the models are not explicitly dependent on the seasonal and regional climate conditions, such as ambient temperature, which in the present work are shown to have a significant impact for BETs.

Some studies propose region-specific case studies to analyze BETs energy consumption and feasibility or compare alternative HDV powertrain technologies based on well-to-wheels GHG emissions and cost of ownership. For example, Mojtaba Lajevardi et al. [15] considered British Columbia, Zhang et al. [16] examined China as a case study, and Middela et al. [17] focused on India. While these studies factor in the impact of the grid energy mix, battery manufacturing, and recycling, on the final GHG emissions and costs, they also acknowledge the sensitivity of the results to the accuracy of the models used for estimating the energy consumption, which do not include region-specific considerations. Recent work by Borlaug et al. [18] and Shoman et al. [19] has addressed the charging requirements for the electrification of heavy-duty trucks. Both studies rely on assumptions for the average energy consumption of electric trucks and use sensitivity analysis to account for the uncertainty of this parameter. In particular, the former work explores the sensitivity of the results when energy consumption is varied between 93 and 174 kWh/100 km (1.5 and 2.8 kWh/mile) with a baseline of 111 kWh/100 km (1.8 kWh/mile), which shows that the daily energy requirements vary significantly. The latter work discusses how the average energy consumption for BETs varies significantly among studies, with values ranging from 120 to 123 kWh/100 km for estimates for 2030, to real-world driving data showing 80–120 kWh/100 km on urban roads and 130–180 kWh/100 km on highways.

The need for numerical simulations to evaluate the energy consumption of BETs emerges from the very limited availability of real-world or experimental data. To the best of the Authors' knowledge, one of the few studies reporting BET experimental data is the work by Sato et al. [20]. The purpose of their study is to quantitatively investigate the energy consumption and energy regeneration rates for medium- and heavy-duty battery-powered electric vehicles that use different driving cycles on a chassis dynamometer.

Zhang et al. [21] utilized a physics-based model for the analysis of energy consumption in a mid-size passenger EV, with the influence of ambient temperature and average driving speed studied on energy efficiency. However, the equations do not explicitly show the dependence of energy consumption on the ambient temperature. In another study by Bai et al. [22], to determine the cost-effectiveness of renewable energy pathways to decarbonize heavy-duty trucks in China, a linear relationship between vehicle energy consumption and vehicle weight was used to estimate the energy requirements of the electrified heavy-duty fleet. Even though the impact of vehicle weight on energy consumption was captured using a simple model, the influence of other geographical factors and weather conditions was excluded.

The presented literature review shows that, although addressing the research questions regarding the feasibility of drayage electrification requires accurate energy consumption models, previous studies often overlook seasonal and geographical impacts, which can have a profound impact on the outcomes of the feasibility analysis. This work aims to fill this gap by developing a detailed vehicle energy consumption model for HD electric trucks to assist in conducting feasibility analysis for electric drayage truck applications.

Models and Validation

A simulation-based analysis is performed in this study to assess the energy requirements of electric drayage trucks and understand the influence of seasonal and regional variations on the total energy consumption. This section presents the proposed energy consumption model for simulating HDVs.

Truck Energy Consumption Model

The vehicles modeled in this study are representative of heavy-duty Class-8 diesel and electric trucks available in the U.S. market. Models for both vehicle types are developed in the MATLAB/Simulink environment using the approach described in Onori et al. [23]. The block diagram of the vehicle simulator is depicted in Figure 3.

The driver model takes as input the upcoming route information and the current vehicle speed to generate the driver commands. The powertrain controller translates the commands into torque requests for the propulsion system, which responds by generating the necessary torque. The generated power is then transmitted to the wheels to overcome road load resistance. Subsequent sections will detail the modeling of the components of the vehicle simulator and the process of route and weather data collection.

Driver Model

The modified Enhanced Driver Model (mEDM) from Shiledar et al. [24] is utilized in this work to emulate the driving behavior of real-world drivers. The mEDM receives route data such as speed limits, road gradients, and traffic conditions to set the target vehicle speed. This model

FIGURE 3 Block diagram of the developed vehicle simulator. The main input is route information; the main output is the resulting energy consumption.

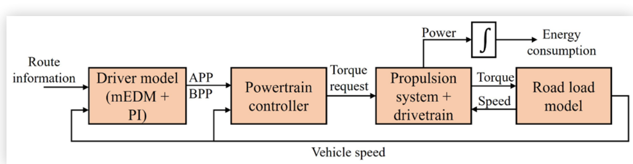

replicates the behavior of a heavy-duty truck driver, including preemptive deceleration before slow-speed road segments to mitigate the high inertia of the vehicle. The mEDM also allows for varying the level of driver aggressiveness (calm, normal, and aggressive) by changing the model parameters, which have been calibrated based on real-world driving data. A proportional-integrator (PI) controller then manages accelerator and brake actions to follow the target speed. The model equations in different driving modes, freeway driving (FD) and safe deceleration (SD), are given below:

$$\frac{d}{dt}v(t)=\begin{cases} a\left[1-\left(\dfrac{v(t)}{v_{sl}(t)-\theta_0}\right)^{\delta}\right], & \text{if } v(t)\le v_{sl}(t)\ [\text{FD}] \\ -b\left[1-\left(\dfrac{v_{sl}(t)-\theta_0}{v(t)}\right)^{\delta}\right], & \text{if } v(t)> v_{sl}(t)\ [\text{FD}] \\ -\dfrac{1}{b}\left(\dfrac{v^2(t)-v_{next}^2}{2s(t)}\right)^2, & \text{if } s(t)\le s_{brake}(t)\ [\text{SD}] \end{cases}$$

$$s_{brake,SS}=\left(1+\frac{c_1}{\delta}\right)\frac{v^2(t)}{2b}$$

$$s_{brake,sl_{change}}=\left(1+\frac{c_1}{\delta}\right)\left(\frac{v^2(t)-v_{sl_{next}}^2}{2b}\right) \tag{1}$$

where v is the vehicle speed, $a(\geq 0)$ is the maximum allowable acceleration, $b(\geq 0)$ is the maximum allowable deceleration, δ is the parameter representing the driver aggressiveness (also referred to as acceleration exponent), v_{sl} is the speed limit on the road, θ_0 is the difference between the actual speed limit and the driver's perceived speed limit, s is the distance to the next obstacle (distance to upcoming stop sign or red traffic light), x_{ego} and x_{next} are the distances between the ego vehicle and the next obstacle (upcoming stop sign/red traffic light: x_{SS} or next speed limit change, $x_{sl_{change}}$). Further, s_{safe} refers to the safe gap from the obstacle that the ego vehicle maintains while it is stationary, and c_1 is the braking aggressiveness, which is a calibration parameter for the critical braking distance s_{brake}, that dictates the switching to safe preemptive deceleration mode. In case of a stop sign, the critical braking distance is given by $s_{brake,SS}$ and for the speed limit change it is given by $s_{brake,\,sl_{change}}$. The speed limit on the portion of road following the speed limit reduction location is given by $v_{sl_{next}}$. Depending on the upcoming obstacle v_{next} can either be zero (if the next obstacle is a stop sign) or $v_{sl_{next}}$ (if there is a speed limit reduction).

The mEDM parameters used for varying the aggressiveness level of heavy-duty truck drivers from [24] are given in Table 1.

TABLE 1 mEDM parameters for varying aggressiveness levels of heavy-duty truck drivers.

mEDM parameter	Calm	Normal	Aggressive
a (m/s^2)	0.29	0.43	0.48
b (m/s^2)	0.38	0.76	0.94
δ (—)	1.73	3.03	3.90
θ_0 (m/s)*	0.57	0.57	0.25
c_1 (—)	0.6	0.32	0.21

* It is assumed that both calm and normal drivers will be comfortable with the same speed offset from the speed limit, whereas the aggressive driver will try to stay closer to it.

Detailed Road Load Model

As far as resistive forces are concerned, only the ones impacting the longitudinal dynamics of the vehicle are included in the simulator. Aerodynamic drag, F_{aero}, rolling resistance, F_{roll}, inertial force, $F_{inertial}$, and grade force, F_{grade}, are the main driving resistances that a truck must overcome. Together, these resistive forces acting on the vehicle are termed the road load, F_{rl} in Equation 2, and are shown in Figure 4.

$$F_{rl}=\underbrace{\frac{1}{2}\rho_a C_d(\phi,\psi)A_f v^2}_{F_{aero}}+\underbrace{MgC_{rr}(T_{tire},v)\cos(\alpha)}_{F_{roll}}+\underbrace{Mg\sin(\alpha)}_{F_{grade}}+\underbrace{M_{eq}\frac{dv}{dt}}_{F_{inertial}}$$

$$T_w=F_{rl}\cdot r_w$$

$$\omega_w=\frac{v}{r_w} \tag{2}$$

where aerodynamic drag depends on air density ρ_a, drag coefficient C_d, vehicle frontal area A_f, and speed v; rolling resistance depends on vehicle mass M, rolling resistance

FIGURE 4 Longitudinal resistive forces on a truck. The vehicle's powertrain will need to generate the tractive or braking forces to counter the resistive forces and achieve a desired vehicle speed.

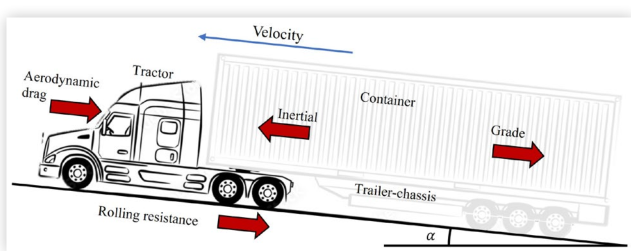

TABLE 2 Summary of BET road load parameters.

Parameter	Value
Vehicle curb mass w/o battery pack (kg)	6930
Frontal area, A_f (m^2)	10
Aerodynamic drag coefficient, C_d (—)	Function of truck configuration and yaw angle with wind
Rolling resistance coefficient, C_{rr} (—)	Function of truck speed and tire shoulder temperature
Wheel radius, r_w (m)	0.483

coefficient C_{rn} and road slope α which is determined based on the elevation profile of the route; grade force depends on vehicle mass and road slope; inertial force depends on equivalent vehicle mass M_{eq} and acceleration dv/dt; g is the gravitational constant, T_w is the total tractive wheel torque provided by the powertrain, ω_w is the wheel angular speed, and r_w is the wheel radius. It is thus critical for estimating energy consumption that these resistive forces are comprehensively modeled. The summary of vehicle road load parameters is given in Table 2.

Aerodynamic Drag Coefficient Model

The truck configuration can be bobtail, tractor-trailer, or tractor-flatbed trailer. Utilizing the data from [25], the aerodynamic drag coefficient, $C_d(\psi, \phi)$, for a conventional heavy-duty truck commonly used in the U.S., is modeled based on various truck configurations, ϕ, and as a function of the relative yaw angle, ψ, with the wind direction. The relative yaw angle with the wind is determined using the following equation from [26],

$$\psi = \left| \tan^{-1}\left(\frac{v_w \sin(\theta_w - \theta_h)}{v + v_w \cos(\theta_w - \theta_h)} \right) \right| \quad (3)$$

where v_w is the wind speed, θ_w and θ_h are the wind and vehicle heading directions, respectively.

Figure 5 shows the yaw-averaged aerodynamic drag coefficient for different configurations of conventional-style trucks, along with the percentage change in aerodynamic drag coefficient observed between the different truck configurations.

Rolling Resistance Coefficient Model

In the vehicle simulator, a detailed transient rolling resistance (RR) model specifically designed and calibrated for

FIGURE 5 Percent reduction in yaw-averaged (0- and 6-degree yaw angles) aerodynamic drag coefficient C_d for different configurations of conventional-style trucks. The drag coefficient can change up to 25.8%, which will directly affect the vehicle's energy consumption.

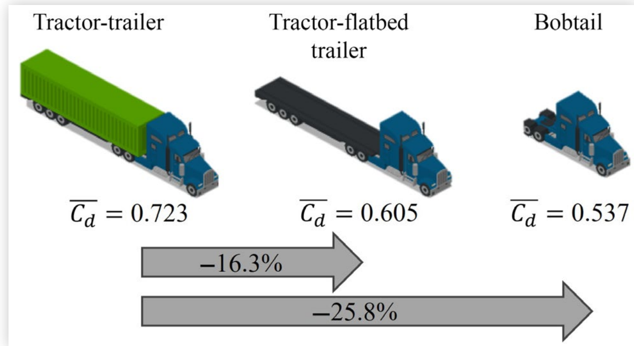

heavy-duty truck tires by Hyttinen et al. [27] is incorporated. This model considers the variation in RR coefficient, $C_{rr}(T_{tire}, v)$, due to tire shoulder temperature, T_{tire}, and vehicle speed. The equations obtained for RR coefficient modeling are given below:

$$\begin{aligned} C_{rr}(T_{tire}, v) &= C_{rr,m}(T_{tire} + \Delta T(v)) \\ C_{rr,m}(T) &= C_{rr,h} + (C_{rr,0} - C_{rr,h}) e^{-\frac{T}{\lambda}} \\ \Delta T(v) &= T_h - (T_0 - T_h)\left(2 - \frac{2}{1 + e^{-\frac{v}{\alpha_v}}}\right) \end{aligned} \quad (4)$$

In the above model, the influence of vehicle speed, v, on the RR coefficient is accounted for by a virtual shift in tire temperature given by $\Delta T(v)$, and the transient RR coefficient is given by the master rolling resistance curve, $C_{rr,m}(T)$. Further, $C_{rr,0}$ represents the RR coefficient at 0°C tire temperature, $C_{rr,h}$, indicates the RR coefficient at elevated temperatures, and λ, the decay parameter that determines the rate at which the RR value transitions from higher to lower values as the tire temperature changes. Furthermore, the tire temperature shift parameters include T_0 and T_h, which denote the temperature shift at zero and high vehicle speeds, respectively, while α_v governs the rate of temperature shift reduction from higher to lower values across varying speeds.

Additionally, a simplified thermal dynamics model for the heating/cooling effects due to the interaction between tire, road surface, and ambient air, T_{amb}, is considered [28]. The thermal dynamics model of tire heating/cooling is given as follows,

$$
\begin{aligned}
&\frac{d}{dt}T_{tire}(t) = -\frac{1}{\tau(v)}\left(T_{tire}(t) - T_{st}(v, T_{amb})\right)\\
&\tau(v) = \tau_h + (\tau_0 - \tau_h)e^{-\frac{v}{\delta_\tau}}\\
&T_{st}(v, T_{amb}) = kv + n_c - (n_c - T_{a,ref})e^{-\frac{v}{\gamma}}\\
&\qquad - (T_{a,ref} - T_{amb})
\end{aligned}
\tag{5}
$$

Where $T_{st}(v, T_{amb})$ is the stabilized tire temperature for a given vehicle speed and ambient temperature, which depends on calibrating multiple factors that include k, n, and γ; $T_{a,ref}$ is the reference ambient temperature where the model is parameterized. Furthermore, $\tau(v)$ is the vehicle speed–dependent thermal time constant. The thermal constant varies between τ_0 when the vehicle is stationary and τ_h for higher vehicle speeds. δ_τ governs the rate of decline from high to low value of the time constant at different speeds.

Electric Truck Powertrain Model

The powertrain of the electric truck is a tandem e-axle configuration, as shown in Figure 6, based on the publicly available information on the Kenworth 6 × 4 T680E. Each e-axle has an electric motor (EM) that can provide a maximum power of 250 kW, and its power conversion efficiency is modeled using a performance map. The EM efficiency map, as shown in Figure 7, is obtained using available EM data from a production vehicle, and is appropriately scaled using the Willans lines approach to match the specification of the modeled HDEV. The EM is connected to a 3-speed gearbox (with gear ratios of 5.6:1, 2.8:1, and 1.4:1). The gearbox, along with the final drive ratio of 2.47:1 and wheel end reduction of 2:1, gives the required torque amplification at the wheels. The model equations for the BET powertrain are given below.

FIGURE 7 Electric machine power conversion efficiency map.

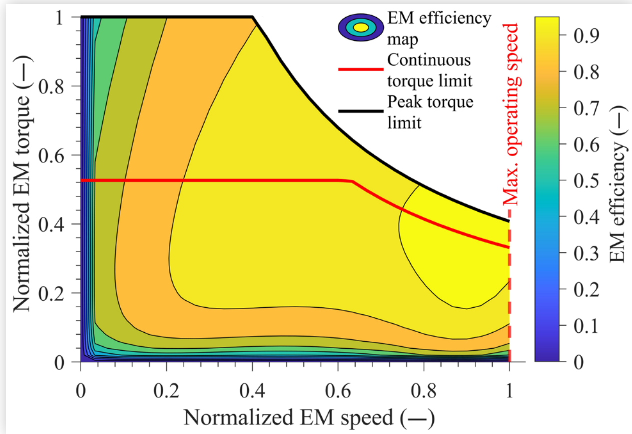

$$
\begin{aligned}
&T_{ax} + T_{br} = T_w\\
&T_{em} = \frac{T_{ax}}{n_e \cdot \lambda_{gb,i} \cdot \lambda_{fd} \cdot \lambda_{we}} \eta_{gb,i}^{\gamma} \cdot \eta_{fd}^{\gamma} \cdot \eta_{we}^{\gamma} \quad \begin{cases} \gamma = 1, & T_{ax} < 0 \\ \gamma = -1, & T_{ax} \geq 0 \end{cases}\\
&\omega_{em} = \omega_w \cdot \lambda_{gb,i} \cdot \lambda_{fd} \cdot \lambda_{we}\\
&P_{em} = T_{em} \cdot \omega_{em} \cdot \eta_{em}^{\gamma}(\omega_{em}, T_{em}) \quad \begin{cases} \gamma = 1, & T_{em} < 0 \\ \gamma = -1, & T_{em} \geq 0 \end{cases}\\
&I_{batt} = \frac{n_e \cdot P_{em} + P_{aux}(T_{amb})}{V_{batt}}
\end{aligned}
\tag{6}
$$

Where T_{ax} is the total axle torque and T_{br} is the total brake torque. T_{em}, ω_{em}, P_{em}, and η_{em} are the EM torque, angular speed, electrical power, and efficiency, respectively; n_e(=2) is the number of e-axles; $\lambda_{gb,i}$ and $\eta_{gb,i}$ are the gear reduction and gear efficiency of ith gear in the gearbox, respectively; λ_{fd} and η_{fd} are the gear reduction and

FIGURE 6 Schematic of the electric truck powertrain including the auxiliary components. EM: Electric Motor, GB: Gearbox, Diff: Differential, HV: High Voltage, LV: Low Voltage, DC/DC: Convertor, DC/AC: Inverter.

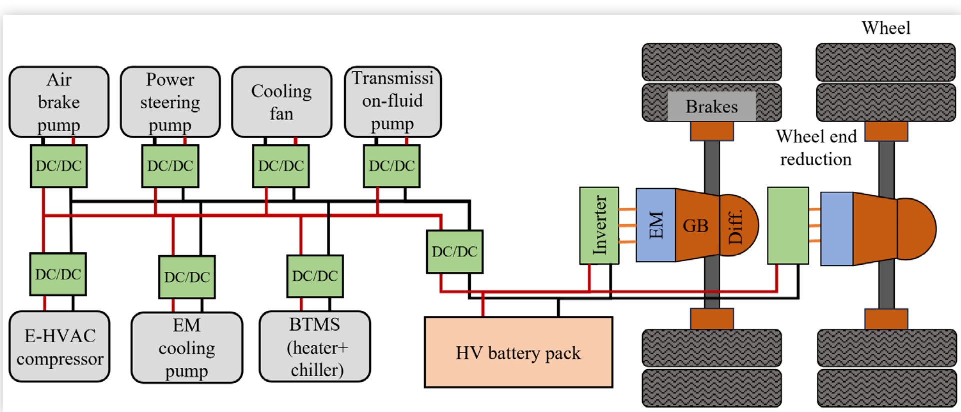

efficiency of the final drive reduction, respectively' λ_{we} and η_{we} being the gear reduction and efficiency of the wheel end reduction; I_{batt} and V_{batt} are the current and terminal voltage of the high-voltage Li-ion battery pack, respectively; $P_{aux}(T_{amb})$ is the total power drawn from the battery pack due to all the electrical auxiliaries. A major advantage of an electric powertrain is the ability to harness kinetic energy during deceleration events, by the process of regenerative braking, where the EM acts as a generator. In this work, a series regenerative braking strategy is employed to maximize the kinetic energy recovery during the braking events, where the EMs provide the braking torque at the wheel until they reach their minimum continuous torque limits. Any braking torque required beyond the EM capacity is met by the service brakes.

The battery pack provides the power to the drivetrain and the energy consumption of the vehicle is determined by integrating a High-Voltage (HV) Li-ion battery model into the simulator. The pack uses LG INR21700-M50T cells, which have NMC-811 material in cathodes and graphite/silicone as anodes [29]. The battery model accounts for cells' electric and thermal dynamics, assuming all cells are identical for modeling, simplifying input/output scaling from cell to pack. Lucero et al. [30] found that neglecting variations in parallel cells minimally impacts pack energy output while significantly reducing the computations. A first-order equivalent circuit model (ECM) of a cell's electrical dynamics [31] is used as given below:

$$
\begin{aligned}
\frac{d}{dt}SoC(t) &= -\frac{I_{cell}(t)}{3600 \cdot Q_{nom}} \\
\frac{d}{dt}V_{RC}(t) &= -\frac{1}{\tau(SoC)}V_{RC}(t) + \frac{1}{C_1(SoC)}I_{cell}(t) \\
V_{cell}(t) &= V_{oc}(SoC) - R_0(SoC) \cdot I_{cell}(t) - V_{RC}(t)
\end{aligned}
\tag{7}
$$

where the battery state-of-charge is SoC, the polarization voltage is V_{RC}, the capacitance is C_1, the relaxation time scale is $\tau(SoC) = R_1(SoC) \cdot C_1(SoC)$, the polarization resistance is $R_1(SoC)$, the high-frequency resistance is R_0, and the cell current is I_{cell}. The ECM parameters are characterized as a function of the battery state-of-charge, using the experimental data collected at a fixed temperature of 23°C [29].

The battery pack is liquid-cooled with a water–glycol–based coolant. The temperature dynamics are modeled using a lumped model approach. The battery pack housing temperature, T_{ho}, and the individual cell temperature, T_{cell}, follow the dynamics as given by the following equation, which is obtained from [32].

$$
\begin{aligned}
C_{cell}\frac{d}{dt}T_{cell}(t) &= I_{cell}(V_{oc} - V_{cell}) + \frac{T_{ho}(t) - T_{cell}(t)}{R_{cell,ho}} \\
C_{ho}\frac{d}{dt}T_{ho}(t) &= N_{cells}\frac{T_{cell}(t) - T_{ho}(t)}{R_{cell,ho}} + \frac{T_{amb}(t) - T_{ho}(t)}{R_{ho,amb}} \\
&\quad -\dot{Q}_{cool} \cdot u_c + \dot{Q}_{heat} \cdot u_h
\end{aligned}
\tag{8}
$$

where C_{cell} and C_{ho} are the lumped thermal capacities of an individual cell and the battery housing, respectively; $R_{cell,ho}$ is the thermal resistance between a single cell and the housing and is assumed to be identical for all the cells; N_{cells} is the total number of cells; $R_{ho,amb}$ is the thermal resistance between the housing and the ambient air. Finally, $\dot{Q}_{cool}$ is the heat removed from the battery during battery cooling, while $\dot{Q}_{heat}$ is the heat added to warm up the battery by the battery thermal management system (BTMS). The variables u_c, $u_h \in \{0,1\}$ are binary variables that control whether the BTMS is cooling or heating the pack housing or is otherwise off. Since all the cells are assumed to be in thermal equilibrium, no term represents the heat transfer between adjacent cells of the pack.

Auxiliary Components Model

Auxiliary components like the BTMS heater and chiller, power steering pump, transmission fluid pump, and pneumatic brakes are vital for HDV function. In conventional trucks, most auxiliary systems are mechanically linked to the engine (by means of belts), so their power usage depends on engine speed. However, in BETs, auxiliaries are independently powered and unaffected by vehicle speed, allowing optimal efficiency. This is most prominent in the case of the HVAC system, where the compressor in a BET is powered by an EM, thus also referred to as E-HVAC. Comprehensive dynamic modeling of auxiliary systems is complex, as the power consumption of different auxiliary components varies by driver, road, weather, and traffic conditions [33]. Weather impacts cabin temperature needs, thereby the HVAC energy consumption. Power for auxiliaries in HDVs can be quite substantial. As all energy in BET comes from batteries, modeling auxiliary power consumption is crucial for accurate energy use estimation. For control applications, detailed models like those in Khuntia et al. [34] for cabin-HVAC or Silvas et al. [35] for power steering are overcomplicated. Instead, a simpler transient model from Gao et al. [36] is used here. Auxiliary loads are modeled with an on/off duty cycle approach. The periods, duty cycles, and nominal operating power of the auxiliary components in the electric truck are given in Table 3. Ambient temperature affects certain auxiliary loads; therefore, it is factored into HVAC and air-brake system loads, as shown in Figure 8. The relationships shown in the figure are based on steady-state load data under various temperatures [37–39]. The HVAC compressor and air-brake pump's duty cycles, originally 50% and 5%, change based on ambient temperature to ensure average power aligns with the temperature-dependent load.

Finally, the water–glycol coolant–based BTMS is modeled separately, considering the thermal model of the battery pack and a simple heuristic-based thermal management strategy developed to maintain the battery temperature within a ±5°C about the desired operating temperature of 25°C. The power consumption of BTMS

TABLE 3 Duty cycle–based modeling approach of electric truck auxiliary component's power consumption.

Auxiliary component	Period (s)	Duty (%)	Nominal operating power (kW)
BTMS	—	—	Battery TD
E-HVAC compressor	150	Amb. TD	2.71
Air-brake pump	100	Amb. TD	2.19
Power steering pump	100	10	3.0
Cooling fan	200	4	5.49
EM cooling pump	—	—	0.16
Transmission fluid pump	—	—	0.5
Electrical load	—	—	0.5

Amb. TD = Ambient temperature dependent; Battery TD = Battery temperature dependent.
The period, duty, and nominal operating power of various auxiliary components are obtained from Gao et al. [36].

heater, P_{heater}, and chiller, $P_{chiller}$, are determined based on the constant value of heat addition and extraction from the housing as well as on the coefficient of performance (COP). The BTMS system COP for heating ($COP_{BTMS,heater}$ = 4) and for cooling ($COP_{BTMS,cooler}$ = 3) are obtained from Teichert et al. [32], and are used in the equation below:

$$P_{heater} = \frac{\dot{Q}_{heat}}{COP_{BTMS,heater}}, \quad P_{chiller} = \frac{\dot{Q}_{cool}}{COP_{BTMS,chiller}} \tag{9}$$

Truck Energy Consumption Model Validation

In addition to the BET powertrain model, the powertrain of a conventional diesel truck is also modeled, with details in the Appendix. Due to the lack of experimental data from heavy-duty electric trucks in operation, the validation of certain subcomponents, such as the comprehensive road load model, is performed using the conventional truck model, as test data is available for heavy-duty conventional trucks in varying weather conditions. Energy consumption model validation uses data from [40], which studied ambient effects on fuel use in commercial vehicles. The study examined the variation in fuel consumption due to seasonal changes in Quebec, Canada. The track test results of a heavy-duty 2017 Freightliner Cascadia truck are used to validate the conventional truck's energy consumption model. The referenced study's truck specs align closely with the conventional truck modeled in this work, differing mainly in model year (2017 vs. 2018) and engine power (410 hp vs. 455 hp). Validating the conventional model supports verification of the HD truck road load model, applicable to both electric and conventional trucks. The tests in the referenced study were recreated in simulations. The test vehicle's weight is set to 24,880 kg and is driven at constant speeds. The average speed, test duration, ambient conditions, and fuel consumption from experiments and simulations are given in Table 4.

Simulated fuel consumption results align closely with experimental data, showing a −0.7% deviation in fall and 2.8% in winter, affirming the proposed model's accuracy for heavy-duty trucks. In both cases, the error remains well within acceptable bounds for energy consumption modeling. The slightly larger error observed in winter may be a result of the additional uncertainties associated with cold-weather conditions (e.g., temperature-dependent powertrain component efficiency changes), which are not captured by the model. However, electric trucks lack sufficient experimental data for system-level validation. Nonetheless, it should be noted that electric truck powertrain component modeling in this study relies on component-level experimental data. The energy consumption of BET under nominal operating conditions, according to the model, ranges between 120 and 180 kWh/100 km, consistent with the literature and the initial tests, as shown in Table 5.

The final validation step is to verify that the BETs can meet the performance requirements for the drayage application. Simulations are conducted to evaluate the performance of the BET compared to the conventional baseline in terms of maximum speed, acceleration times, gradability, and stability specifications for an HD truck in drayage applications. The results of the performance validation are tabulated in Table 6.

The performance of the electric truck is similar to or exceeds that of the conventional truck and can meet the performance requirements of the HDV performance for drayage application, as reported in the CALSTART report [45]. It is important to acknowledge that the validation of the BET presented above lacks direct system-level verification, unlike that conducted for the conventional truck. In the absence of detailed experimental data required for comprehensive validation, a comparison of energy consumption variations with ranges reported in the literature is employed as a sanity check.

FIGURE 8 Ambient temperature dependence of HVAC system load (left) and air-brake system load (right).

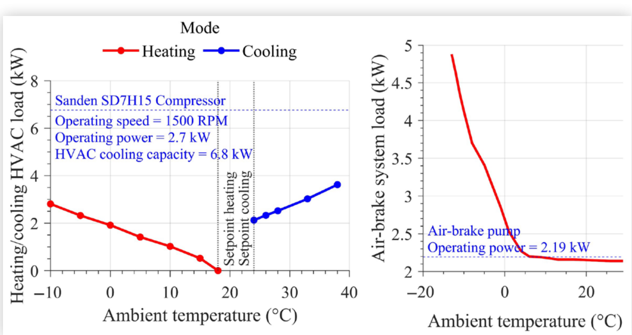

TABLE 4 Test conditions and vehicle energy consumption model validation for conventional truck.

Season	Fall		Winter	
Vehicle speed (km/h)	105		90	
Test run length (km)	100		90	
Ambient temperature (°C)	15.4		−6.3	
Air density (kg/m^3)	1.245		1.337	
Average fuel use	**Exp.**	**Sim.**	**Exp.**	**Sim.**
Consumed fuel (kg)	29.45	29.65	27.76	26.98
Fuel consumption (L/100 km)	35.27	35.51	36.94	35.90
Experiment and simulation error (%)	−0.7%		2.8%	

TABLE 5 Validation of electric truck energy consumption.

Source	Energy consumption (kWh/100 km)	Method
Sato et al. [20]	126–148	Experimental
Ragon [41]	90–150	Experimental
NACFE RoL report [42]	159	Experimental
CARB report [43]	120–148	Experimental
Mansour et al. [44]	138	Simulation
This article	120–180	Simulation

Routes and Weather Data Gathering

This section details the procedure followed to obtain the operating domain characterization for the drayage truck application case study presented in this work. To understand the energy requirements of drayage trucks, the first data acquired is the route origins and destinations (OD) that these trucks are expected to travel on in a year in a specific region. The route ODs are obtained using the process described by Sujan et al. [46], which takes into account the freight movement collected using the Streetlight data. The route ODs for the drayage trucks operating in the Port of Savannah, GA, are identified separately by month and for both the inbound and outbound travel directions to/from the port. Figure 9 shows the major origin and destination locations for inbound and outbound travel to/from the port, in different months of the year 2021, respectively.

Using Google and HERE Routing, the trips to and from the Port of Savannah, GA, for each OD location are mapped, including route data like latitude, longitude, distance, speed limits, and elevation. Subsequently, local weather conditions along these routes are collected, emphasizing the impact of weather on vehicle energy use, with ambient temperature and air density as key factors, as given in Equations 1–8. National Oceanic and Atmospheric Administration (NOAA)—Meteorological Assimilation Data Ingest System (MADIS) data and the method from [47] are employed to calculate variations of ambient temperature and air density for each latitude and longitude coordinate pairs along the route. Consistent 2021 weather data is used, sampled for 3 days each month—a hot, cold, and nominal day—selected to represent significant weather variability. Further, the sampling of weather conditions on the route is conducted at a specific time of the day only, which in this case is selected to be noon, as it coincides with the peak time of travel.

TABLE 6 Performance comparison of conventional and electric trucks.

Powertrain	Drayage application requirements [45]	Conv. truck	Elec. truck
Maximum speed (km/h)	≥100	129.5	141.9
Acceleration 0–48 km/h time (s)	Must be sufficient to operate on local roads and highways	13	12
Acceleration 48–80 km/h time (s)		23	21
Acceleration 80–96 km/h time (s)		24	17
Gradeability 1% (km/h)	No specific requirements	121.9	135.7
Gradeability 2% (km/h)		90.8	118.1
Gradeability 6% (km/h)	64	60.2	67.6
Startability (%) [EM continuous torque limit]	≥6	35	17
Startability (%) [EM peak torque limit]	≥6	35	34

FIGURE 9 Locations of monthly inbound routes' origins (left) and outbound routes' destinations (right) for drayage routes at the Port of Savannah, GA.

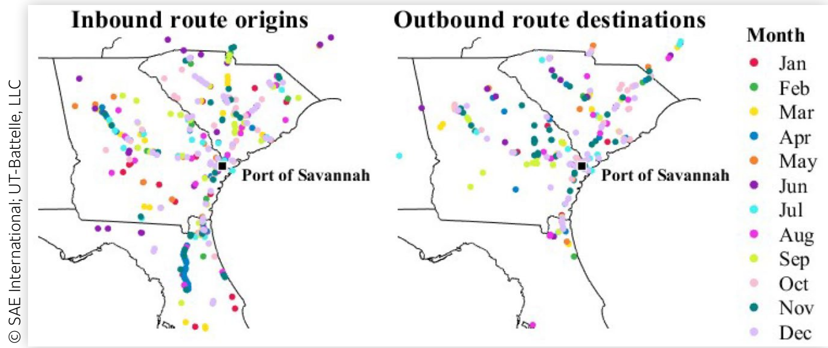

Doing so, temperature changes over the route with respect to time are lost, but the computational burden during the simulation runtime is significantly reduced, while still accounting for maximum variability in weather conditions. The process for identifying the dates to obtain the representative days for weather data gathering for a given route is provided in the Appendix. Figure 10 illustrates the monthly average route ambient temperature and air density changes on cold, nominal, and hot days for all the routes in the region around the port of interest. In addition to this, the bottom box plot shows monthly temperature variation per day type.

FIGURE 10 Monthly weather condition variations in the region around the Port of Savannah, GA. Each month is characterized by average route temperature (top) and average route air density (middle) for cold, nominal, and hot representative days. The distributions show the variations over the various routes. The box plots (bottom) show the fraction of days that fall within each day type for each month.

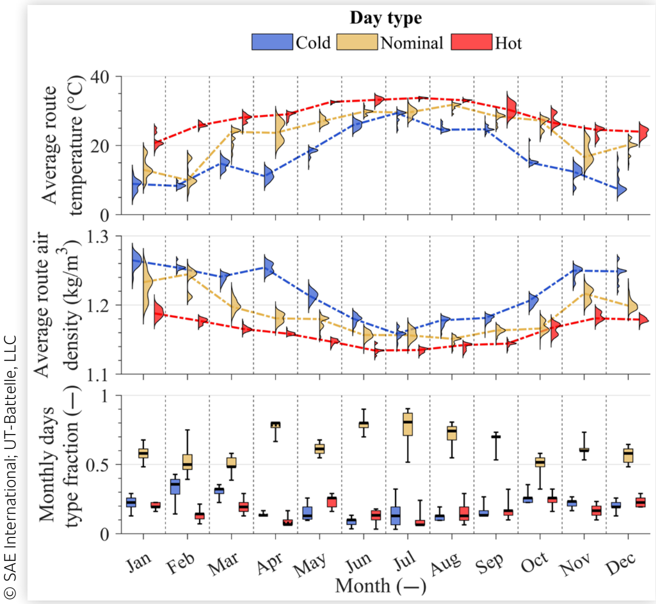

The region of the Port of Savannah, GA, experiences a humid subtropical climate, characterized by brief, mild winters, and prolonged, hot summers. Weather conditions can change significantly based on route and season. Air density varies by approximately 10% when comparing the coldest winter days (November–February) to the hottest summer days (June–August). Route temperatures range from 4°C to approximately 35°C. These fluctuations impact road load, affecting aerodynamic drag directly via air density and RR indirectly through ambient temperature. Auxiliaries' power consumption is also affected by ambient temperature, impacting total auxiliary power consumption. Similarly, the routes and weather data for the Port of Houston, TX, and the Port of Tacoma, WA, are obtained.

A comprehensive simulation study is conducted using these weather conditions and different routes as variables in previously developed vehicle models to analyze energy consumption, revealing seasonal or geographical trends.

Results and Discussion

In this section, the results of the simulation study are presented. The large-scale simulations required for this regional-level analysis are conducted using the high-performance computing resources of the Ohio Supercomputer Center [48]. Access to a large number of processing cores (CPU) on the supercomputer enables parallel execution of simulations across different combinations of routes, weather conditions, and vehicle weights, significantly reducing the total time required to complete the analysis. Simulating a 200 km route for one vehicle takes under 45 seconds on a typical CPU (e.g., AMD Ryzen 9 5900HX). However, running millions of simulations as required by the analysis in this study and in future technoeconomic analyses becomes a significant bottleneck. High-performance resources, such as those at the Ohio Supercomputer Center, minimize analysis time by parallelizing simulations across multiple CPU cores; yet, using 200 cores, the evaluation of the energy consumption of the trucks for one port still demands about half a day of simulations.

Total Energy Consumption Variations due to Geographical and Seasonal Variations

First, the inbound and outbound routes in the Port of Savannah, GA region, as shown in Figure 9, are grouped together to form different groups. The inbound and outbound routes are clustered into 15 groups based on their proximity to one another, as shown in Figure 11. Route grouping is carried out using K-medoids clustering, with the Haversine formula used as the distance metric to cluster geographically proximate route ODs. The Haversine formulation computes the shortest surface distance between two points given their latitude and longitude. K-medoids is preferred over K-means, as it allows the use of non-Euclidean distance metrics like Haversine distance and ensures that cluster centers (medoids) are actual data points rather than average centroids, making it better suited for this application. Finally, ODs outside the 16 km (~10 mile) radius circle around the medoid of the corresponding group are removed from the group to ensure only the route ODs that are indeed geographically closely located are within a group.

Since not all routes are covered by the trucks every month, grouping the routes allows for analyzing the influence of weather variations on energy consumption to travel to (from) different locations around the Port of Savannah, GA, throughout the year. The groups are numbered in ascending order based on the group center distance from the port. Additionally, the marker colors in the maps represent the observed elevation changes relative to the port. The peak elevation change is around ±300 m in the region around the port among all the routes. The group average speed limit is also shown in the same figure. Investigating the energy consumption of travel to and from different route groups to the port enables an in-depth study of how geographical route conditions affect energy usage. Specifically, groups 1, 5, 6, 7, and 12 are of particular interest for both inbound and outbound routes. Routes in group 1 are the shortest, have negligible elevation change, and feature the lowest average speed limit among all the route groups. Groups 5, 6, and 7 have routes of similar distances but differ in elevation changes and average speed limits. For instance, groups 5 and 6 have similar elevation changes; however, the average speed limit for routes in group 5 is ~75 km/h, which is significantly lower than the ~100 km/h average speed limit for routes in group 6. Conversely, groups 6 and 7 have similar average speed limits, but group 6 routes experience significant elevation changes while group 7 routes have practically none. Finally, group 12 consists of the longest routes with the maximum elevation change. Comparing energy consumption across these routes aids in understanding the impacts of geographical and seasonal factors.

The influence of geographical and seasonal variations on the energy consumption of a drayage truck over a year is illustrated in Figure 12 for three vehicle weights, 13.6, 27.2, and 36.3 tons, representing the light, nominal,

FIGURE 11 Inbound (left) and outbound (route) route grouping for analyzing the impact of geographical and weather variation on energy consumption in HD trucks at Port of Savannah, GA. The maps show the location of origins and destinations with the color scale indicating the elevation change. The charts at the bottom show the group average route speed limit, with the color scale indicating the median route distance.

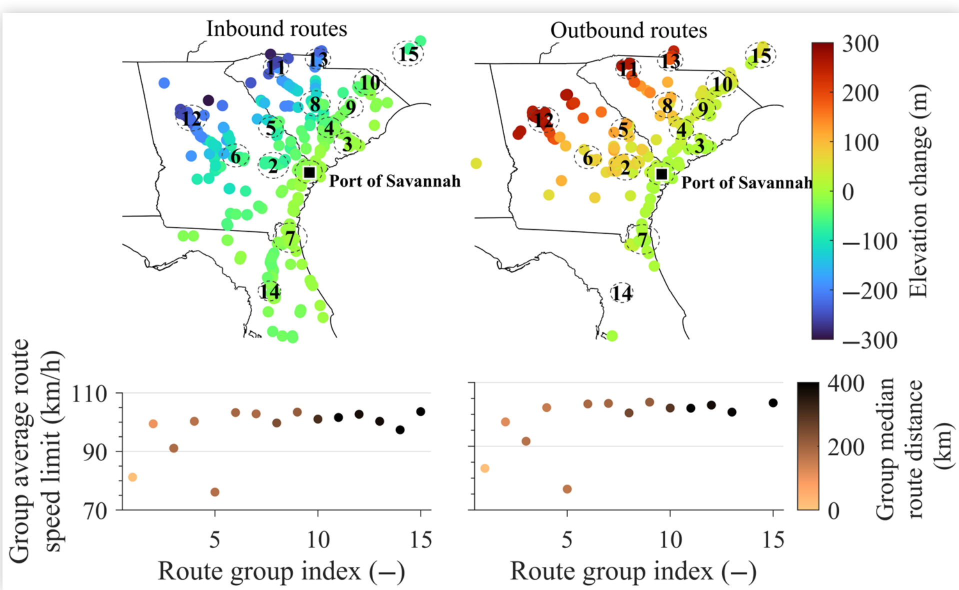

FIGURE 12 Electric energy consumption variation of electric drayage trucks due to geographical and seasonal variations on different inbound and outbound route groups for three vehicle weights at Port of Savannah, GA.

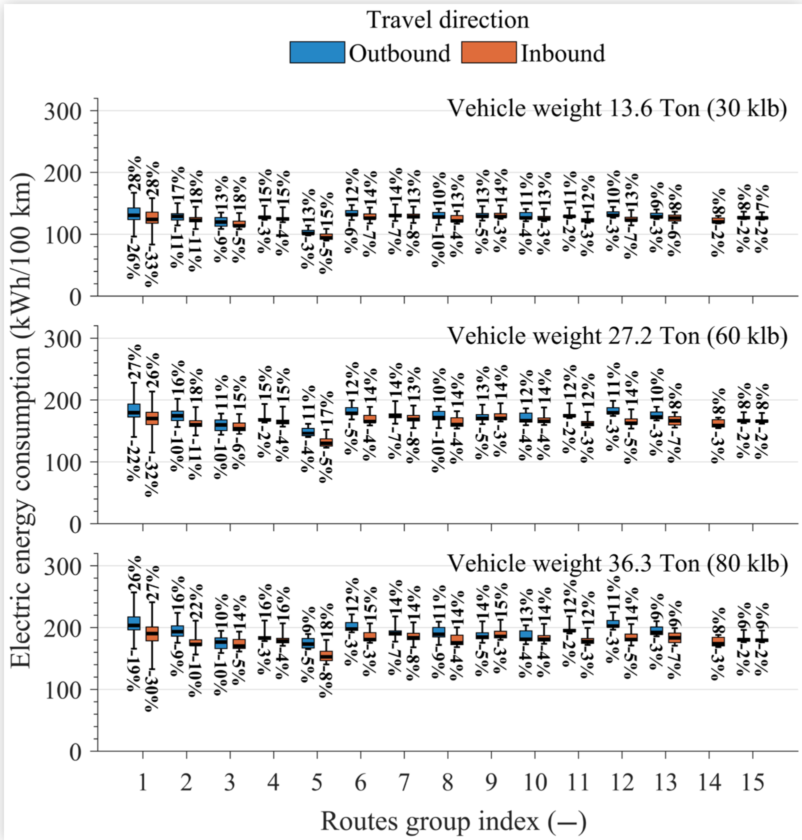

and full payload conditions likely experienced by the electric drayage trucks. As expected, with an increase in vehicle weight, the energy consumption increases when driving over the same routes. Electric energy consumption on longer routes, like for route group 12, varies by −7% to 14% from the median, while shorter routes like the route group 1, show a variation of −33% to 28% depending on the vehicle weight. Additionally, energy consumption is slightly higher on outbound routes compared to inbound routes. This can be attributed to the relative change in elevation between the start and end points of the respective trips. Since the port is located at sea level, inbound trips in general experience a net negative elevation change, while outbound trips encounter a positive elevation change.

As previously noted, shifts in seasonal weather conditions result in yearly energy consumption variations. Figure 13 outlines how monthly weather differences influence energy use across identical routes for electric trucks weighing 27.2 tons, specifically focusing on route groups 5, 6, and 7. The displayed data highlights a distinct pattern in seasonal energy consumption, with vehicles using more energy during the colder winter months than in the warm summer months. Furthermore, electricity consumption tends to fluctuate more during winter. For example, in December, route group 6 experiences electricity consumption variations ranging from −24% to 26% of the month's median consumption. Conversely, in July, the variation is notably lower, from −2% to 1%. This disparity can be attributed to the considerable fluctuation in average temperatures during December, which can swing from 5°C to 30°C, contrasting with the more stable July temperatures, which only vary from 25°C to 35°C.

Figure 13 can be further utilized to evaluate the impact of geographical factors such as speed limit and elevation. As shown in Figure 11, route group 5 has the lowest average speed limit among route groups 5, 6, and 7. Consequently, route group 5 exhibits the lowest energy consumption throughout the year. With the truck speed constrained by the road speed limit, vehicles travel the slowest on route group 5, reducing aerodynamic drag and RR, which are highly sensitive to speed. When comparing route groups 6 and 7, which are similar in all aspects except elevation change, it is observed that energy consumption is lower on route group 7 than on route group 6 for both inbound and outbound trips; however, when analyzing the electric energy consumption on the same route groups, the negative elevation changes on inbound trips for route group 6 provide significant opportunities for regenerative braking. This reduces the

FIGURE 13 Month-wise electric energy consumption variation of electric trucks on route groups 5, 6, and 7 due to differences in weather conditions in each month at Port of Savannah, GA, for a 27.2 Ton vehicle.

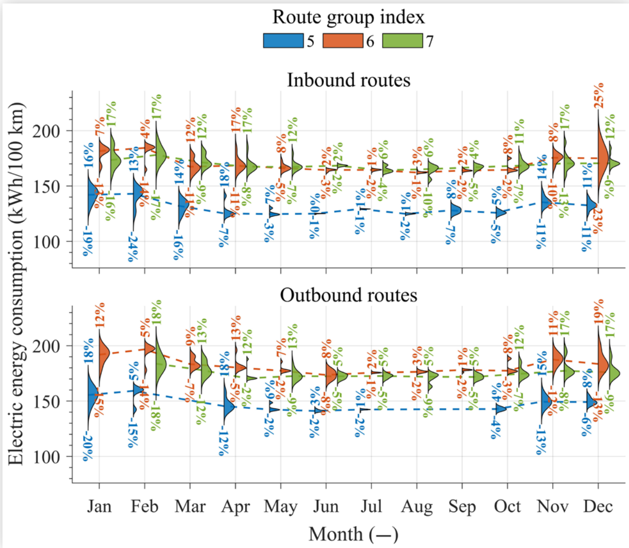

difference in electricity consumption between route groups 6 and 7. In contrast, the benefit of regenerative braking energy diminishes when traveling on the outbound trips on the same route groups.

Variations in Auxiliary Power Consumption due to Seasonal Variability

The simulation results also allow for an analysis of the impact of seasonal variations on auxiliary power consumption for electric trucks. Figure 14 depicts the distribution of average auxiliary consumption in different months of the year, categorized by day type. The major auxiliaries in the electric truck are the BTMS and HVAC, both of which are influenced by the ambient temperature. The auxiliary power consumption is lowest during the time of spring (March–May) and fall (September–October), where the temperatures are moderate, 16°C to 26°C, such that both HVAC and BTMS systems are not required for maintaining the desired cabin and battery temperature during operation. Conversely, higher auxiliary power consumption is observed during the coldest days of winter months as well as during the hottest days of summer months, with the maximum being for winter months.

For the cold days in the month of January, where temperature ranges between 5°C and 15°C, the BTMS heater is used to warm up the battery and the HVAC system is used to heat up the cabin; however, the BTMS heater forms a major fraction (60%–80%) of the total auxiliary power consumption during the coldest days of the year as seen from Figure 15. Similarly, the BTMS chiller is required to cool down the battery and has the biggest contribution to total auxiliary consumption on the hot days of July, with HVAC contribution coming in second after the BTMS chiller during the hottest time of the year, when temperatures can go over 32°C.

FIGURE 14 Electric truck average total auxiliary power consumption for different months and representative temperature day types at Port of Savannah, GA.

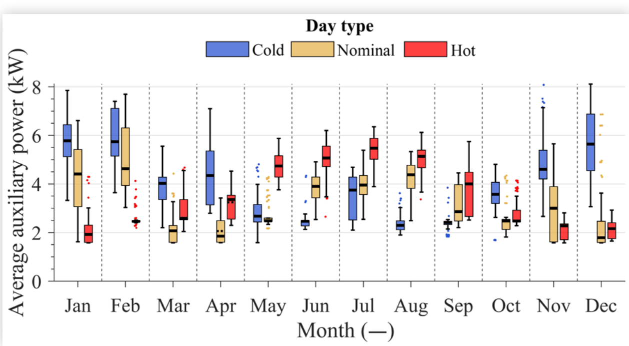

FIGURE 15 Contribution of different auxiliary components to the total auxiliary power consumption for trucks operating in various months (January, April, July, and August) in the Port of Savannah region. The columns represent the different temperature days—cold, nominal, and hot in the respective months.

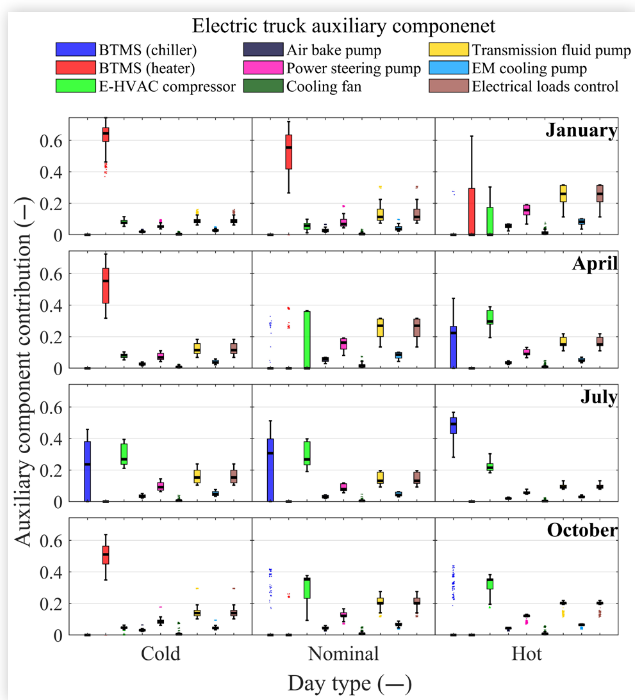

Drayage Truck Energy Consumption and Auxiliary Power Consumption Variability Across Distinct Ports

A similar analysis was conducted for two additional ports with significantly different weather and geographical conditions: the Port of Houston, TX, and the Port of Tacoma, WA. These ports were selected to capture the impact of contrasting climates, humid subtropical in Houston and cold maritime in Tacoma, on vehicle energy consumption. Additionally, the region of Tacoma is highly mountainous, which can result in drastic elevation changes over the routes as compared to the other two regions, which have moderate elevation change overall. Comparing the energy consumption results of a 27.2 Ton electric truck from all three ports offers valuable insights into the variations in energy consumption that electric drayage trucks are likely to encounter under different environmental and operational conditions. The variation in energy consumption at these ports as a function of average route ambient temperature for both inbound and outbound routes in the respective regions is shown in Figure 16.

Each dot on the graph represents the energy consumption for a certain trip. The solid lines represent the average trend line. The probability of trips with a certain energy consumption and average ambient temperature is compactly shown in the distribution graphs on the right and top sides, respectively. In general, energy consumption tends to increase as the average ambient temperature drops across the three port regions. Trucks operating near the Port of Tacoma, WA, consume more energy than those in the other two port areas. This can be attributed to the colder climate in Tacoma, which causes energy consumption to increase compared to the other ports. The highest and lowest energy consumption figures are also noted for trucks in this region, with peaks exceeding 350 kWh/100 km on certain outbound routes with significant elevation gain in cold conditions and lows around 100 kWh/100 km on particular inbound routes with marked elevation drop in milder temperatures. The Port of Savannah, GA, and Port of Houston, TX, regions exhibit similar energy consumption patterns for trucks, ranging from 150 to 200 kWh/100 km for 27.2 Ton trucks, due to their comparable average ambient temperatures on the routes. This analysis underscores the shortcomings of using a simplified, fixed energy consumption rate for BETs as seen in some previous studies, which can lead to inaccurate results if regional geographic and climatic variances are not taken into account.

Similarly, the impact of ambient temperature conditions on auxiliary power use at these specific ports is compared, as illustrated in Figure 17. Given that auxiliary power usage is chiefly influenced by ambient temperature, the scatter plots depicting truck auxiliary power consumption from the three ports show significant overlap. The notable differences arise when examining the distributions of average auxiliary power at these ports. As previously stated, HVAC and BTMS are the largest consumers of power among all auxiliaries, mainly active during cold temperatures. The climate around the Port of Tacoma, WA, is predominantly cold for most of the year, leading to consistently higher auxiliary power consumption.

FIGURE 16 Comparison of electric energy consumption of 27.2 Ton electric drayage trucks operating on routes in three distinct ports. Each dot on the graph represents the energy consumption for a certain trip. The solid lines represent the average trend line. The probability of trips with a certain energy consumption and average ambient temperature is compactly shown in the distribution graphs on the right and top sides, respectively.

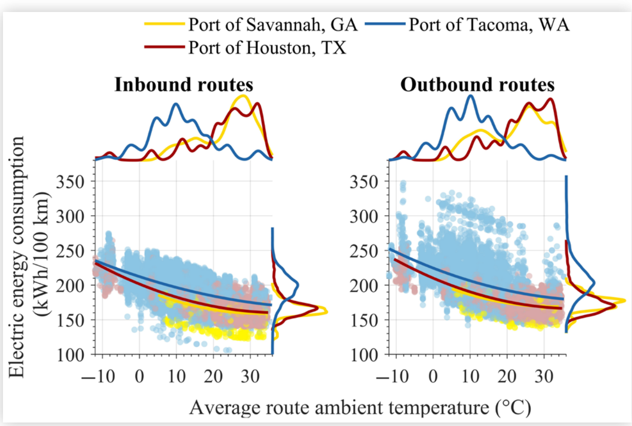

FIGURE 17 Comparison of auxiliary power consumptions in electric drayage trucks operating on routes in three distinct ports. Each dot on the graph represents the average auxiliary power for a certain trip. The solid lines represent the average trend line. The probability of trips with a certain average auxiliary power and average ambient temperature is compactly shown in the distribution graphs on the right and top sides, respectively.

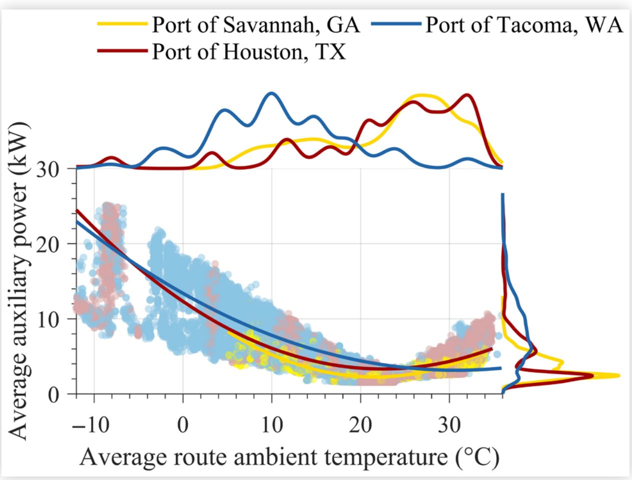

Conversely, at both the Port of Savannah, GA, and the Port of Houston, TX, auxiliary power consumption tends to be lower since HVAC and BTMS operate minimally between 16°C and 26°C, which is the average temperature range for those regions. However, the Port of Houston, TX, occasionally faces severe cold temperatures in winter, dropping to as little as −10°C, resulting in increased power demand from auxiliaries, especially HVAC and BTMS.

Impact of Geographical and Meteorological Conditions and Driver Style on Driving Range and Payload Capacity of Electric Drayage Trucks

A simulation case study was executed on a smaller scale to explore how various factors affecting vehicle energy consumption impact the driving range of BETs. The study involved running simulations of battery electric drayage trucks on selected outbound routes across three different regions. Outbound routes were chosen for this investigation because they typically exhibit higher energy usage than inbound routes, leading to more pronounced range limitations, which this analysis aims to address. Initially, outbound routes in each port region were categorized by the average ambient temperature. Within these categories, short routes overlapping with more than 95% redundancy with a longer route were eliminated. By reducing overlap, the analysis retained a set of relatively longer routes for conducting the simulation study aimed at assessing the effects on driving range. For each average ambient temperature group, simulations were performed, adjusting variables such as vehicle weight (by modifying cargo load with half-load at 11.3 Ton (25 k lb) and 22.6 Ton (50 k lb) as full load), battery size of 400 kWh, and driver behavior (calm, normal, and aggressive). A 400-kWh battery pack was selected as it aligns with the specs of currently available BETs [49]. In each simulation scenario, the drayage truck, with a curb weight of 9.42 tonnes including the battery pack, starts with a battery SoC of 95%. The simulation continues until the truck either completes its route or its battery is completely drained. Examining these simulation results offers insights into how geography, weather, and driver behavior influence the driving range of electric drayage trucks. The study also highlights how weather, particularly ambient temperature, affects the driving range at the three ports, as depicted in Figure 18. Results are presented for scenarios with drivers of normal aggressiveness, with comparable outcomes for other levels of driving style.

Overall, the driving range on outbound routes in the three port areas declines as the ambient temperature drops. There is an approximate 2.4% reduction for every 6°C decrease in temperature, for both full and half payloads. As anticipated, full payload conditions result in a noticeably shorter range than half payload conditions. At identical

FIGURE 18 Maximum driving range variation of a 400-kWh electric drayage truck on outbound routes in three distinct ports with full battery at the beginning of the port for different average ambient temperature ranges. The driver's aggressiveness level is normal. Driving range is determined for two payload weights of 11.3 and 22.6 tons, representing half and full load conditions, respectively, generally expected for these drayage trucks.

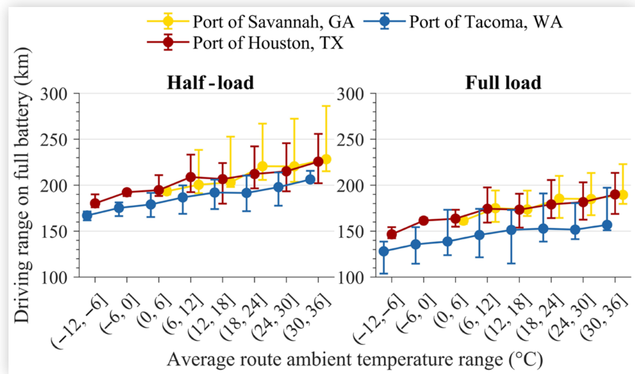

ambient temperatures, Tacoma's outbound routes exhibit a driving range about 20–25 km lower than routes at Houston and Savannah, likely due to Tacoma's mountainous terrain causing increased energy consumption. This emphasizes the influence of positive road gradients on reducing the driving range of BETs. For Savannah's drayage operations, a 400 kWh battery under full load reaches only about 180 km, well below the usual 400 km range. With half loads, the range is around 225 km, reaching up to 290 km on some routes. However, electric trucks can't complete all drayage routes, even half-loaded. Extending the range would require larger batteries (800–1000 kWh), but this reduces payload capacity and raises costs. Similar trends are observed at the other two ports. Interestingly, for the Port of Savannah, larger error bars can be observed, in particular at half-load conditions (see Figure 18). This larger range variability can be attributed to the geography. Since the range is computed based on the outbound routes, certain routes that go inland toward Atlanta have a significant elevation gain, resulting in higher energy demand and lower range. On the other hand, routes along the coastline have little to no elevation change, and thus lower energy demand and significantly longer driving range.

Next, the influence of driver aggressiveness on the driving range of the battery electric drayage truck is determined. In Figure 19, the driving range of a 400-kWh electric drayage truck in an 18°C–24°C ambient temperature range when driven by drivers with three levels of driver aggressiveness is illustrated.

A calm driver achieves the greatest range in both loading scenarios across the three ports, surpassing the normal driver and then the aggressive driver. In the Savannah and Houston ports, a calm driver can extend the range by about 8% compared to a normal driver, while an

FIGURE 19 Maximum driving range variation of a 400-kWh electric drayage truck on outbound routes in three distinct ports with full battery in the beginning at the port for different driver aggressiveness levels in 18°C–24°C range of average route ambient temperature. Same payload conditions as used in the previous figure.

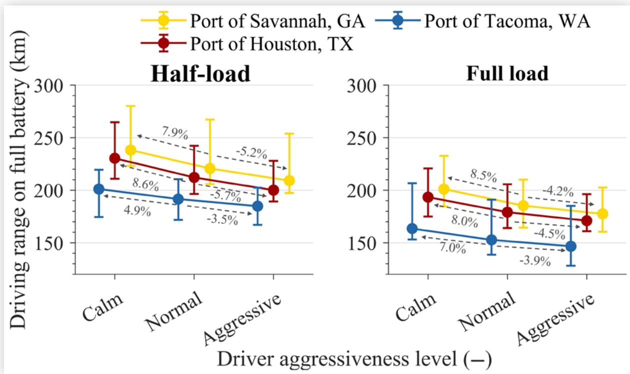

aggressive driver reduces the range by 4%–5%. In contrast, at the Port of Tacoma, WA, calm driving increases range by 5% with a half payload and by 7% with a full payload. The higher road grade in Tacoma may explain the disparity, as it affects the range more than driver behavior. Still, driver behavior significantly influences the truck's maximum range.

Conclusions

Because of varying geography and weather conditions at each port, adopting BETs in drayage port operations requires a custom technoeconomic assessment of converting diesel drayage fleets. A detailed simulation framework for estimating the energy use of electric HDVs is crucial for reliable analysis, replacing generic kWh/100 km values with accurate, local estimates. This study proposes a vehicle simulator for electric trucks, accounting for geographic and weather impacts on energy use, validated with limited real-world data, which can be utilized to obtain local energy consumption statistics. Due to scarce operational data on seasonal energy use in electric trucks, a bottom-up modeling approach is necessary, although it limits full model validation. Collaboration with industry partners is underway to acquire top-down operational data for further detailed validation.

The simulation-based analysis shows significant effects of seasonal and geographic factors on BETs energy consumption. Ambient temperature affects aerodynamic drag, RR, and auxiliary power, notably HVAC and BTMS in cold weather. Elevation changes and route speeds also impact the energy usage in BETs, with negative elevations benefiting BETs as regenerative braking can be utilized to recoup kinetic energy. The simulation also examines how these factors, along with driver aggressiveness and battery size, affect payload capacity and range of electric drayage trucks across U.S. ports.

As pointed out earlier, running large-scale analyses as those presented in this work requires access to high computational resources like the Ohio Supercomputer Center. To reduce reliance on such computing facilities, efforts are being focused on creating a simpler model using regression-based machine learning to estimate vehicle energy consumption with minimal route and weather information, which will be quicker and easier to integrate with pre-existing technoeconomic tools. Future work aims to cover more U.S. ports to guide electric truck adoption in drayage fleets without disrupting operations. Also, the focus will be to explore additional battery chemistries to identify the best lithium-ion options for heavy-duty use, especially in drayage. Using detailed semi-empirical battery aging models, the battery capacity degradation and need for battery replacements in BETs in drayage applications will be analyzed. Furthermore, future work utilizing the OR-AGENT framework will evaluate total ownership costs by integrating the truck energy consumption model with the battery and truck daily operation models.

Disclaimer

Acknowledgements

This research was supported by the US Department of Energy (DOE), Office of Critical Minerals & Energy Innovation, Transportation Technologies Office under award WBS 7.2.0.502 / FWP CEVT442, administered by Oak Ridge National Laboratory's National Transportation Research Center. The DOE technical management team included Laura Roberson, Patrick Walsh, Raphael Isaac, and Casey Roepke. The authors thank the support from sponsors and remain solely responsible for the content and opinions expressed.

Declaration of AI-Assisted Technologies

The authors declare that no generative AI technologies were used in the preparation and writing of this article. In doing so, the authors take full responsibility for the authenticity and scientific integrity of this article.

Contact Information

Manfredi Villani, PhD, corresponding author
Assistant Professor
Department of Mechanical and Aerospace Engineering
E447 Scott Lab 201 W. 19th Avenue, Columbus, OH 43210
villani.5@osu.edu

Definitions, Acronyms, Abbreviations

BETs - battery electric trucks
BTMS - battery thermal management system
ECM - equivalent circuit model
GHG - greenhouse gases
HD - heavy duty
HDEV - heavy-duty electric vehicle
HDV - heavy-duty vehicle
HVAC - heating, ventilation, and air-conditioning
LDV - light-duty vehicle
mEDM - modified enhanced driver model
MC - Monte Carlo
OD - origin–destination
RR - rolling resistance
SoC - state-of-charge
TCO - total cost of ownership
VMT - vehicle miles travelled
ZEV - zero-emissions vehicle

References

1. U.S. Department of Transportation, "Bureau of Transportation Statistics, Freight Facts and Figures," Washington, DC, 2022, https://data.bts.gov/stories/s/Moving-Goods-in-the-United-States/bcyt-rqmu/
2. U.S. Department of Energy, "September H_2IQ Hour: Decarbonizing Heavy-Duty Vehicles," 2023, https://www.energy.gov/sites/default/files/2023-10/h2iqhour-09212023.pdf
3. U.S. Environmental Protection Agency, "Global Greenhouse Gas Overview," 2024, https://www.epa.gov/ghgemissions/global-greenhouse-gas-overview
4. U.S. Energy Information Administration (EIA), "U.S. Energy-Related CO_2 Emissions Fell 1.7% in 2016," 2016, https://www.eia.gov/todayinenergy/detail.php?id=30712#
5. Sugihara, C., Hardman, S., and Kurani, K., "Who Decides Which Trucks to Buy? Implications for Electrifying Freight Fleets," *Transportation Research Part D: Transport and Environment* 126 (2024): 104015, doi:https://doi.org/10.1016/j.trd.2023.104015.
6. Villani, M., Pandolfi, A., Ahmed, Q., and Pianese, C., "Data-Driven Vehicle Specification of Conventional and Electric Heavy-Duty Commercial Trucks for Improved Energy Consumption," *SAE Int. J. Commer. Veh.* 18, no. 3 (2025): 371-389, doi:https://doi.org/10.4271/02-18-03-0018.
7. Sujan, V.A., Sun, R., and Snyder, I., "Or-Agent Framework – Architecting Electrified Heavy-Duty Drayage Applications," *Applied Energy* 386 (2025): 125540, doi:https://doi.org/10.1016/j.apenergy.2025.125540.
8. Demir E., Bektas T., and Laporte G., "A Review of Recent Research on Green Road Freight Transportation," *European Journal of Operational Research*, vol. 237, pp. 775-793, 2014, doi:https://doi.org/10.1016/j.ejor.2013.12.033.
9. Golbasi, O. and Kina, E., "Haul Truck Fuel Consumption Modeling under Random Operating Conditions: A Case Study," *Transportation Research Part D: Transport and Environment* 102 (2022): 103135, doi:https://doi.org/10.1016/j.trd.2021.103135.
10. Giuliano, G., Dessouky, M., Dexter, S., Fang, J. et al., "Heavy-Duty Trucks: The Challenge of Getting to Zero," *Transportation Research Part D: Transport and Environment* 93 (2021): 102742, doi:https://doi.org/10.1016/j.trd.2021.102742.
11. Tanvir, S., Un-Noor, F., Boriboonsomsin, K., and Gao, Z., "Feasibility of Operating a Heavy-Duty Battery Electric Truck Fleet for Drayage Applications," *Transportation Research Record* 2675, no. 1 (2021): 258-268, doi:https://doi.org/10.1177/0361198120957325.
12. Kotz, A., Kelly, K., Lustbader, J., Cary, S. et al., "Port of New York and New Jersey Drayage Electrification Analysis," National Renewable Energy Laboratory (NREL), Tech. Rep., 2022, www.nrel.gov/publications.
13. Hunter, C., Penev, M., Reznicek, E., Lustbader, J. et al., "Spatial and Temporal Analysis of the Total Cost of Ownership for Class 8 Tractors and Class 4 Parcel Delivery Trucks," National Renewable Energy Laboratory (NREL), Tech. Rep., 2021, https://www.osti.gov/servlets/purl/1821615/%0Ahttps://www.nrel.gov/docs/fy21osti/71796.pdf.

14. Brooker, A., Gonder, J., Wang, L., Wood, E. et al., "Fastsim: A Model to Estimate Vehicle Efficiency, Cost and Performance," SAE Technical Paper 2015-01-0973 (2015), doi:https://doi.org/10.4271/2015-01-0973.
15. Lajevardi, S.M., Axsen, J., and Crawford, C., "Comparing Alternative Heavy-Duty Drivetrains Based on GHG Emissions, Ownership and Abatement Costs: Simulations of Freight Routes in British Columbia," *Transportation Research Part D: Transport and Environment* 76 (2019): 19-55, doi:https://doi.org/10.1016/j.trd.2019.08.031.
16. Zhang, X., Lin, Z., Crawford, C., and Li, S., "Techno-Economic Comparison of Electrification for Heavy-Duty Trucks in China by 2040," *Transportation Research Part D: Transport and Environment* 102 (2022): 103152, doi:https://doi.org/10.1016/j.trd.2021.103152.
17. Middela, M.S., Mahesh, S., Kancharla, S.R., Ramadurai, G. et al., "Complete LCA of Battery Electric and Conventional Fuel Vehicles for Freight Trips," *Transportation Research Part D: Transport and Environment* 110 (2022): 103398, doi:https://doi.org/10.1016/j.trd.2022.103398.
18. Borlaug B., Muratori M., Gilleran M., Woody D., Muston W., Canada T., Ingram A., Gresham H., and McQueen C., "Heavy-Duty Truck Electrification and the Impacts of Depot Charging on Electricity Distribution Systems," *Nature Energy*, vol. 6, pp. 673-682, 6 2021, doi:https://doi.org/10.1038/s41560-021-00855-0.
19. Shoman, W., Yeh, S., Sprei, F., Plötz, P. et al., "Battery Electric Long-Haul Trucks in Europe: Public Charging, Energy, and Power Requirements," *Transportation Research Part D: Transport and Environment* 121 (2023): 103825, doi:https://doi.org/10.1016/j.trd.2023.103825.
20. Sato, S., Jiang, Y.J., Russell, R.L., Miller, J.W. et al., "Experimental Driving Performance Evaluation of Battery-Powered Medium and Heavy Duty All-Electric Vehicles," *International Journal of Electrical Power and Energy Systems* 141 (2022): 10, doi:https://doi.org/10.1016/j.ijepes.2022.108100.
21. Zhang, C., Kotz, A., Kelly, K., and Rippelmeyer, L., "Development of Heavy-Duty Vehicle Representative Driving Cycles via Decision Tree Regression," *Transportation Research Part D: Transport and Environment* 95 (2021): 102843, doi:https://doi.org/10.1016/j.trd.2021.102843.
22. Bai, F., Zhao, F., Liu, X., Liu, Z. et al., "A Cost-Effectiveness Comparison of Renewable Energy Pathways for Decarbonizing Heavy-Duty Vehicles in China," *Energy Conversion and Management* 322 (2024): 119111, doi:https://doi.org/10.1016/j.enconman.2024.119111.
23. Onori, S., Serrao, L., and Rizzoni, G., *Hybrid Electric Vehicles: Energy Management Strategies* (London: Springer Publishing Company, 2016), 1-112, doi:https://doi.org/10.1007/978-1-4471-6781-5
24. Shiledar, A., Villani, M., Rizzoni, G., Adinolfi, E.A. et al., "A Modified Enhanced Driver Model for Heavy-Duty Vehicles with Safe Deceleration," SAE Technical Paper 2023-24-0171 (2023), doi:https://doi.org/10.4271/2023-24-0171.
25. Vegendla, P., Saha, R., Sofu, T., and Hwang, L.K., "Comparison of Aerodynamic Drag and Underhood Thermal Analysis of Two Heavy-Duty Vehicles," *International Journal of Aerodynamics* 5 (2016): 105, doi:https://doi.org/10.1504/IJAD.2016.080532.
26. Howell, J.P., "Aerodynamic Drag in a Windy Environment," in *The International Vehicle Aerodynamics Conference*, Holywell Park, Loughborough, UK, 2014, 19-30, Woodhead Publishing, https://doi.org/10.1533/9780081002452.1.19.
27. Hyttinen J., Ussner M., Österlöf R., Jerrelind J., and Drugge L., "Effect of Ambient and Tyre Temperature on Truck Tyre Rolling Resistance," *International Journal of Automotive Technology*, vol. 23, pp. 1651-1661, 12 2022, doi:https://doi.org/10.1007/s12239-022-0143-6.
28. Hyttinen, J., Ussner, M., Österlöf, R., Jerrelind, J. et al., "Truck Tyre Transient Rolling Resistance and Temperature at Varying Vehicle Velocities—Measurements and Simulations," *Polymer Testing* 122 (2023): 108004, doi:https://doi.org/10.1016/j.polymertesting.2023.108004.
29. Pozzato, G., Allam, A., and Onori, S., "Lithium-Ion Battery Aging Dataset Based on Electric Vehicle Real-Driving Profiles," *Data in Brief* 41 (2022): 4, doi:https://doi.org/10.1016/j.dib.2022.107995.
30. Lucero, J.N.E., Sujan, V.A., and Onori, S., "An Experimentally Validated Electro-Thermal EV Battery Pack Model Incorporating Cycle-Life Aging and Cell-to-Cell Variations," *IEEE Transactions on Transportation Electrification* 10, no. 4 (2024): 8122-8136, doi:https://doi.org/10.1109/TTE.2024.3365028.
31. Plett, G., *Battery Management Systems, Volume I: Battery Modeling* (Boston, MA: Artech, 2015)
32. Teichert, O., Schneider, J., and Lienkamp, M., "Strategy Beats Power: Cooling System Design for Battery-Electric Long-Haul Trucks," in *35th International Electric Vehicle Symposium and Exhibition (EVS35)*, Oslo, Norway, 2022.
33. Andersson, C., "On Auxiliary Systems in Commercial Vehicles," Ph.D. dissertation, Lund Institute of Technology, 2004, accessed June 24, 2026, https://lucris.lub.lu.se/ws/files/5907461/716038.pdf.
34. Khuntia, S., Hanif, A., Singh, S.P., and Ahmed, Q., "Control Oriented Model of Cabin-HVAC System in a Long-Haul Trucks for Energy Management Applications," SAE Technical Paper 2022-01-0179 (2022), doi:https://doi.org/10.4271/2022-01-0179.
35. Silvas, E., Turan, O., Hofman, T., and Steinbuch, M., "Modeling for Control and Optimal Design of a Power Steering Pump and an Air Conditioning Compressor Used in Heavy Duty Trucks," in *2013 IEEE Vehicle Power and Propulsion Conference (VPPC)*, Beijing, China, 2013, 1-6.
36. Gao, Z., Finney, C., Daw, C., LaClair, T.J. et al., "Comparative Study of Hybrid Powertrains on Fuel Saving, Emissions, and Component Energy Loss in HD Trucks," *SAE Int. J. Commer. Veh.* 7, no. 2 (2014): 414-431, doi:https://doi.org/10.4271/2014-01-2326.

37. Li, K., Luo, S., Fan, L., Hu, S. et al., "Investigation on the Performance and Characteristics of a Heat Pump System for Electric Vehicles under Extreme Temperature Conditions," *Case Studies in Thermal Engineering* 27 (2021): 101308, doi:https://doi.org/10.1016/j.csite.2021.101308.
38. Okaeme, C., Lustbader, J., Sigler, C., Jorgensen, I. et al., "Cabin Thermal Management Analysis for Supertruck II Next-Generation Hybrid Electric Truck Design," *SAE Int. J. Commer. Veh.* 14, no. 3 (2021): 271-288, doi:https://doi.org/10.4271/02-14-03-0022.
39. Sjostedt, C.-J., Wikander, J., and Flemmer, H., "Evaluation of Auxiliary Device Efficiency in Heavy Vehicle Application," in *International Design Engineering Technical Conferences and Computers and Information in Engineering Conference*, Portland, OR, 2013. American Society of Mechanical Engineers, doi:https://doi.org/10.1115/DETC2013-13395.
40. Surcel, M.D., "Evaluation of the Effect of Ambient Conditions on the Fuel Consumption of Commercial Vehicles," SAE Technical Paper 2022-01-0528 (2022), doi:https://doi.org/10.4271/2022-01-0528.
41. Ragon, P.-L., "Real-World Use Cases for Zero-Emission Trucks: Heavy Tractor-Trailers for Goods Transport in the European Union," Tech. Rep., August 2025.
42. North American Council for Freight Efficiency (NACFE), "Electric Trucks Have Arrived: The Use Case for Heavy-Duty Regional Haul Tractors," North American Council for Freight Efficiency (NACFE), Tech. Rep., 2022, https://nacfe.org/research/run-on-less/run-on-less-electric/hd-regional-haul-tractors/#top
43. California Air Resources Board (CARB), "Battery Electric Truck and Bus Energy Efficiency," California Air Resources Board (CARB), Tech. Rep., 2018, https://ww2.arb.ca.gov/sites/default/files/2018-11/180124hdbevefficiency.pdf
44. Mansour, C., Bou Gebrael, J., Kancharla, A., Freyermuth, V. et al., "Energy Price Sensitivity and Cost Analysis of Battery Electric and Fuel Cell Powertrains for Class 8 Heavy-Duty Trucks in Real-World Scenarios: A 2024, 2035, and 2050 Perspective," SAE Technical Paper 2025-01-8592 (2025), doi:https://doi.org/10.4271/2025-01-8592.
45. Papson, A. and Ippoliti, M., "Key Performance Parameters for Drayage Trucks Operating at the Ports of Los Angeles and Long Beach," CALSTART, Pasadena, CA, 2013.
46. Sujan, V., Sun, R., Jatana, G., and Fan, J., "Hydrogen and Electric Charging Infrastructure for Heavy-Duty Trucks: A Nationally Scalable Megaregion Assessment," SAE Technical Paper 2025-01-8608 (2025), doi:https://doi.org/10.4271/2025-01-8608.
47. Moore, A., Siekmann, A., and Sujan, V., "Spatio-Temporal and Weather Characterization of Road Loads of Electrified Heavy-Duty Commercial Vehicles Across U.S. Interstate Roads," Oak Ridge National Laboratory (ORNL), Oak Ridge, TN, 2023, https://www.osti.gov/biblio/1995692.
48. Ohio Supercomputer Center, 1987, Ohio Supercomputer Center. Columbus OH: Ohio Supercomputer Center, accessed June 24, 2026, https://ror.org/01apna436.
49. EESI, "Fact Sheet | The Future of the Trucking Industry: Electric Semi-Trucks," 2023, https://www.eesi.org/papers/view/fact-sheet-the-future-of-the-trucking-industry-electric-semi-trucks-2023.

Appendix: Supplemental Modeling Details

Conventional Truck Energy Consumption Model

The powertrain of the conventional truck, as illustrated in Figure A.1, consists of a 339.2 kW (455hp) diesel-powered

FIGURE A.1 Schematic of the conventional truck powertrain including auxiliary components. GB: gearbox; Diff.: differential gear; LV: low voltage.

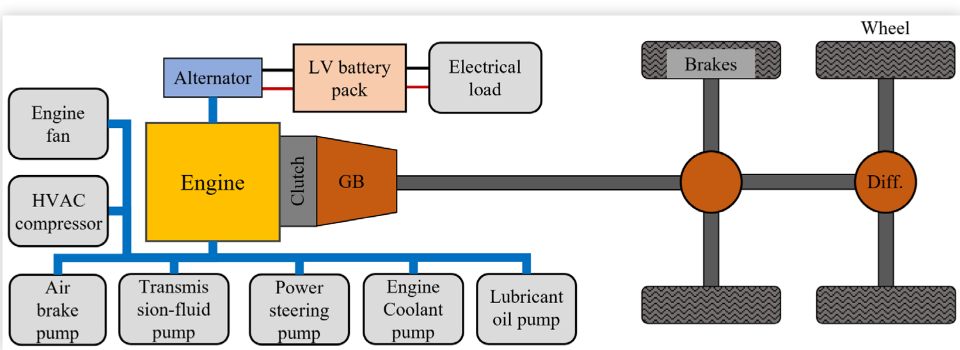

FIGURE A.2 Normalized engine fuel consumption map.

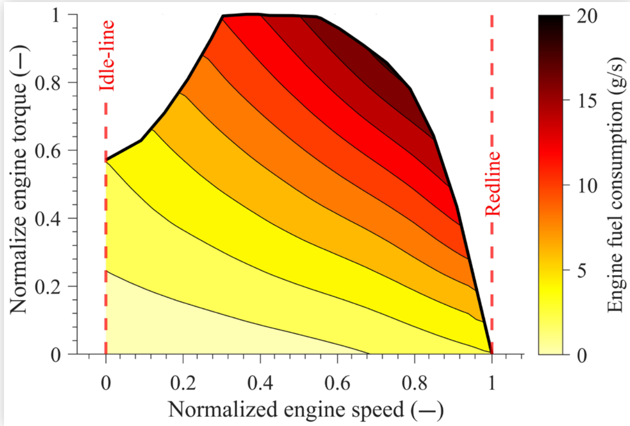

engine from the 2018 model year with a 10-speed automatic manual transmission and a final rear drive reduction of 2.64:1 at the differential.

The engine fuel consumption map, as shown in Figure A.2, is obtained from the EPA Greenhouse Gas Emissions Models vehicle simulator, while the transmission gear ratios and efficiencies are obtained from the Eaton Fuller 10-speed transmission specification sheet. The truck specifications have been selected to be representative of real trucks used in drayage operations. The model equations for the conventional truck powertrain are given below.

$$
\begin{aligned}
&T_{ax} + T_{br} = T_w \\
&T_{eng} = \frac{T_{ax}}{\lambda_{gb,i} \cdot \lambda_{fd}} \eta_{gb,i}^{\gamma} \cdot \eta_{fd}^{\gamma} + T_{aux}\left(T_{amb}\right) \begin{cases} \gamma = 1 & T_{ax} < 0 \\ \gamma = -1 & T_{ax} \geq 0 \end{cases} \\
&\omega_{eng} = \omega_w \cdot \lambda_{gb,i} \cdot \lambda_{fd} \\
&\dot{m}_f = \dot{m}_f\left(\omega_{eng}, T_{eng}\right)
\end{aligned} \tag{A.1}
$$

where T_{ax} is the total axle torque and T_{br} is the total brake torque. T_{eng} and ω_{eng} are the engine torque and angular speed, respectively. $\lambda_{gb,i}$ and $\eta_{gb,i}$ are the gear reduction and gear efficiency of the i-th gear in the gearbox, respectively, while λ_{fd} and η_{fd} are the gear reduction and efficiency of the final drive reduction, respectively. $T_{aux}(T_{amb})$ is the additional torque required to power the auxiliaries. Finally, $\dot{m}_f$ is the fuel consumption rate of the engine.

The auxiliary components are modeled using the same duty cycle-based approach as followed for the electric truck auxiliaries modeling. The details of the period and the duty of various auxiliary components are given in Table A.1. Since most of the auxiliaries in a conventional truck are mechanically coupled to the engine, their operating power depends on the engine speed.

Determination of Representative Days for Route Weather Data Collection

A separate data set containing the daily average temperature of all the major cities along all the identified routes is created. Next, for each route, for the corresponding month it belongs to, a route temperature vector is constructed for all the days of the month using Equation (A.2). The elements of the route temperature vector are the average temperature (in units of K) of all N major cities along the route on that day. For each route, the D count of the route temperature vector is created, where D equals the total days for the corresponding month.

$$
T_{route,i} = \left[T_{1,i} \cdots T_{N,i}\right]^T \quad i = 1,\ldots,D \tag{A.2}
$$

TABLE A.1 Duty-cycle based modelling of conventional truck auxiliary components' power consumption.

Auxiliary component	Period (s)	Duty (%)	Operating power as a function of engine speed (kW)				
Engine fan	200	5	0.71	2.36	7.56	16.73	29.81
HVAC compressor	150	Amb. TD	1.03	2.45	3.83	5.27	6.67
Air-brake pump	100	Amb. TD	1.0	1.69	2.53	3.51	4.51
Power steering pump	100	10	3.04	5.52	8.04	10.47	12.99
Engine coolant pump	-	-	0.0	0.22	0.56	1.25	1.88
Lubricant oil pump	-	-	0.14	1.24	2.05	3.24	4.97
Transmission fluid pump	-	-	0.5				
Electrical load	-	-	0.6				
	Engine speed (RPM)		500	1000	1500	2000	2500

Amb. TD = Ambient temperature dependent

This is followed by calculating the representative route temperature for the day as follows:

$$\overline{T_{route,i}} = \sqrt{\frac{1}{N}\sum_{k=1}^{N} T_{k,i}^2} \tag{A.3}$$

Using this representative route temperature, the hottest, the coldest, and nominal (median) temperature dates of the months for the concerned route are determined as follows:

$$\begin{aligned} i_{hot} &= \arg\max_i \overline{T_{route,i}} \\ i_{cold} &= \arg\max_i \overline{T_{route,i}} \\ i_{nominal} &= \arg\max_i \left(\left| \text{median}\left(\overline{T_{route,1:D}}\right) - \overline{T_{route,i}} \right| \right) \end{aligned} \tag{A.4}$$

here, median($\overline{T_{route,1:D}}$) is the median representative temperature of the route for the given month.

Finally, the weather data consisting of ambient temperature, air density, wind speed, and wind direction for each route is obtained for the three representative days.